Influence of water on the electronic structure of metal-supported graphene: Insights from van der Waals density functional theory

Xiao Li (李晓),[1] Ji Feng (冯济),[1,*] Enge Wang (王恩哥),[1] Sheng Meng (孟胜),[2] Jiří Klimeš,[3] and Angelos Michaelides[3]

[1]*International Center for Quantum Materials, School of Physics, Peking University, Beijing 100871, China*

[2]*Institute of Physics, Chinese Academy of Sciences, Beijing 100190, China*

[3]*London Centre for Nanotechnology and Department of Chemistry, University College London, London WC1E 6BT, UK*

(Received 10 November 2011; revised manuscript received 10 January 2012; published 21 February 2012)

We investigate the interaction between water and metal-supported graphene through van der Waals density functional theory calculations. Our results show a systematic increase in the adsorption energy of water on graphene in the presence of underlying metal substrates. In addition, we find that the electronic nature of the graphene-metal contacts behave differently upon water adsorption: In the case of a weak, physical graphene-metal contact, the charge carrier doping level of graphene is tuned by water, resulting in a Fermi level shift on the order of ∼100 meV. In the case of a strong chemical graphene-metal contact, the π and π^* bands of graphene are hardly perturbed by water adsorption. These results illustrate the correlated nature of the interactions between water, graphene, and metal substrates, and show that the electronic structure and the doping level of graphene can be tailored by water deposition.

DOI: 10.1103/PhysRevB.85.085425 PACS number(s): 68.43.Fg, 73.20.At, 73.22.Pr, 79.60.Dp

I. INTRODUCTION

Graphene monolayers have been prepared routinely on a variety of metal surfaces,[1–3] producing highly ordered, millimeter-scale, continuous stripes. Graphene-metal contacts, as either independent functional devices or key components for integrating graphene-based devices into more traditional circuits, are potentially important for developing next-generation electronics.[4–7] Depending on the interaction strength, graphene-metal contacts can be divided into two categories: The first group consists of Ni, Co, Ru, and Pd surfaces which bind graphene strongly, and the second group including Cu, Ag, Au, Pt, and Al binds graphene rather weakly. These two cases exhibit quite different characteristics in electronic structure and carrier transport,[5,8–11] with Ni(111) and Cu(111) surfaces as respective representatives.[10,12] When graphene makes contact with metal surfaces, moiré superstructures are often formed as a result of lattice mismatch between graphene and the underlying metal surfaces, which represent suitable templates for growing and stabilizing nanostructures.[12–15] For instance, xenon forms isolated two-dimensional (2D) patches each comprising tens of xenon atoms on the underlying moiré superstructures of graphene/Ru(0001).[15]

Thanks to these attractive properties and the great incentive for developing nanoelectronics, graphene/metal interfaces have been intensively investigated with tremendous effort devoted to understanding the functionality and the electronic nature of graphene-metal interfaces. One of the foremost challenges is to introduce charge carrier doping of graphene in a controllable manner for better performance in electronic, optical, and catalytic applications. Traditionally, this is achieved by changing the metal substrate to modify the electronic structure of graphene.[5,11] However, progress in this direction has been dominated by incremental discoveries rather than by the more desirable rational design. In this regard, a detailed and quantitative understanding of the electronic interaction between metal surfaces and graphene, possibly including additional adsorbates, is much needed. Since water is ubiquitous in nature, as well as in fabrication and utilization of nanodevices, the interaction between water and graphene-metal contacts is of practical importance during the synthesis and routine use of graphene-based devices.

In this paper we show that the electronic interaction and the charge carrier doping level of graphene on metal surfaces are modified by water adsorption, and sensitive to the orientation of the water adlayer structures. Our results show that water adsorption on graphene is enhanced (adsorption energy increased by up to 30%) in the presence of the underlying metal substrates. Our calculations reveal the specific role of the metal substrates: They provide a nearly-free electron gas in the vicinity of graphene, which enhances the induced electron density of graphene in response to the dipole of adsorbed water. In addition, different types of graphene-metal contact respond differently to water adsorption: In the case of a weak graphene-metal contact, the charge carrier doping level of graphene is tuned by water, resulting in a Fermi level shift of ∼100 meV. In the case of a strong chemical graphene-metal contact, the π and π^* bands of graphene are nearly unperturbed by water adsorption. In contrast, the isolated graphene and its doping level are insensitive to water adsorption. These results illustrate that it is viable to tailor the electronic structure of graphene by polar adsorbate (water in this case) deposition.

II. METHODS

We use first-principles density functional theory (DFT) calculations to investigate the geometric and electronic structure of water adsorption on graphene/metal surfaces. The Vienna ab initio simulation package (VASP)[16,17] with projector augmented wave (PAW) potentials[18] and a plane-wave cutoff of 500 eV, is employed. We utilize the Monkhorst-Pack **k**-point meshes[19] of at least $20 \times 20 \times 1$ per (1×1) surface unit cell to perform the Brillouin zone summation. Mean-field dipole corrections along the direction perpendicular to the surface are included in the total energy.[20,21]

A vital role is played by van der Waals (vdW) interactions for graphene-metal contacts[22] and water physisorption.[23] Since long-range correlation is not adequately captured in popular generalized gradient corrected (GGA) exchange-correlation functionals, we have employed various methods to include the relatively weak vdW interaction in our first-principles calculations. These include (i) the DFT-D3 method[24] with the revised PBE (revPBE) exchange-correlation functional, for which, a semiempirical term, E^{D3}, is added to account for vdW interactions; and (ii) a modified version of vdW-DF, referred to as "optB86b-vdW,"[25,26] in which the revPBE exchange functional of the original vdW-DF of Dion *et al.*,[27] is replaced with the optB86b exchange functional to yield more accurate equilibrium interatomic distances and energies for a wide range of systems. This functional has recently been implemented in VASP by Klimeš *et al.*[26] following the scheme of Roman-Perez and Soler.[28] For comparison we also use the pure PBE exchange-correlation functional[29] without any explicit vdW correction. As we will show below, among the three methods optB86b-vdW offers the best performance when compared to experiments. Therefore, the main results and discussions herein are based on optB86b-vdW.

We choose Ni(111) and Cu(111) as representative metal substrates to study strong and weak graphene-metal interactions, respectively. To make a clean comparison between the three different methods, with and without vdW corrections, we use the experimental lattice constants of Ni and Cu after effects of zero-point anharmonic expansion have been removed, namely, 3.508 Å for Ni and 3.596 Å for Cu.[30] Since the lattice constants of the (111) surfaces (2.48 Å for Ni and 2.54 Å for Cu) are very close to that of the graphene ($\sqrt{3} \times \sqrt{3}$) lattice (2.46 Å), it allows us to use rather small supercells to model the graphene-metal contacts without having to introduce significant artificial strain. For the same reason, these two surfaces do not produce moiré patterns in most cases, except when there is an orientational mismatch between graphene and the substrate.[31] Slabs of four atomic layers separated by 22 Å of vacuum are used to model the metal surfaces, with atoms in the bottom two layers fixed at their respective bulk positions during structural relaxations. Graphene is placed on one side of the slab, on which water is then adsorbed. Spin polarization is taken into account for systems with Ni. Structure optimizations are performed with a convergence threshold of 0.01 eV/Å on the interatomic forces. As a reference, water on isolated graphene is also calculated with the lattice constant of graphene being 2.466 Å; this is the optimized value obtained with optB86b-vdW. As a benchmark, we have performed calculations with a higher (700 eV) plane-wave cutoff, and harder PAW potentials for metal elements explicitly treating the p electrons as valence. This more accurate calculation yielded adsorption energies differing only by <2 meV compared to those using PAW potentials which treat the p electrons in the pseudized core.

The binding energy between graphene and the metal substrate is obtained from

$$E_{\text{G-M}} = (E^{\text{tot}}[\text{G/M}] - E^{\text{tot}}[\text{M}] - E^{\text{tot}}[\text{G}])/n. \quad (1)$$

The adsorption energy of water is calculated as

$$E_{\text{ads}} = (E^{\text{tot}}[\text{H}_2\text{O-G/M}] - E^{\text{tot}}[\text{G/M}] - mE^{\text{tot}}[\text{H}_2\text{O}])/m. \quad (2)$$

Here, E^{tot}[G/M] and E^{tot}[H_2O-G/M] are the total energies per supercell of the graphene/metal and water-graphene/metal systems, respectively. E^{tot}[M], E^{tot}[G], and E^{tot} [H_2O] are those for the clean metal surface slab, free-standing graphene, and an isolated water molecule, respectively. The isolated water molecule reference energy has been computed in a 20 Å × 20 Å × 20 Å cell. Integers n and m are the numbers of C atoms and water molecules in the supercell, respectively.

The nonlocal correlation energy, E^{nlc}, as given in Dion *et al.*[27] is evaluated in the calculation of the total energy. Therefore, the corresponding attraction due to nonlocal correlation in the binding energy for graphene on the metal surfaces can be obtained from

$$E^{\text{nlc}}_{\text{G-M}} = (E^{\text{nlc}}[\text{G/M}] - E^{\text{nlc}}[\text{M}] - E^{\text{nlc}}[\text{G}])/n. \quad (3)$$

The nonlocal correlation contributions in other adsorption systems can be obtained in a similar manner.

To analyze the nature of the water-graphene/metal interaction, we have examined electron density differences at the interface, $\Delta\rho(\mathbf{r})$, and the planar-averaged density difference, $\Delta\rho^{\text{avg}}(z)$, as well as the projected density of states (PDOS) and band structures of the systems. Here $\Delta\rho$ is defined as

$$\Delta\rho = \rho[\text{G/M}] - \rho[M] - \rho[G], \quad (4)$$

$$\Delta\rho = \rho[\text{H}_2\text{O-G}] - \rho[\text{G}] - \rho[\text{H}_2\text{O}], \quad (5)$$

and

$$\Delta\rho = \rho[\text{H}_2\text{O-G/M}] - \rho[\text{G/M}] - \rho[\text{H}_2\text{O}], \quad (6)$$

for graphene on a metal surface, water on graphene, and water on graphene/metal, respectively. Here, ρ[G/M], ρ[H_2O-G], and ρ[H_2O-G/M] are the electron densities of the graphene/metal system, the water-graphene system and the water-graphene/metal system, respectively. ρ[M], ρ[G], and ρ[H_2O] are those for the clean metal surface, free-standing graphene, and the isolated water molecule, respectively. The density differences are calculated on identical structures (i.e., with the same structures as in the adsorption state). The planar-averaged electron density difference $\Delta\rho^{\text{avg}}(z)$ is obtained from

$$\Delta\rho^{\text{avg}}(z) = \int_{\Sigma(z)} dxdy\Delta\rho(x,y,z), \quad (7)$$

where the z axis is along the surface normal direction and where $\Sigma(z)$ is the cross-section of the supercell in the x-y plane at z.

III. RESULTS AND DISCUSSIONS

A. Metal-supported graphene

Before studying water adsorption, we first look at the interaction between graphene and the metal surfaces. Taking Ni(111) as an example, there are three possible arrangements of the atomic positions at the graphene/metal interface: top-fcc (TF for short), top-hcp (TH), and fcc-hcp (FH), which are named according to the positions of the carbon atoms projected onto the metal surface lattice, shown in Fig. 1. In the TF

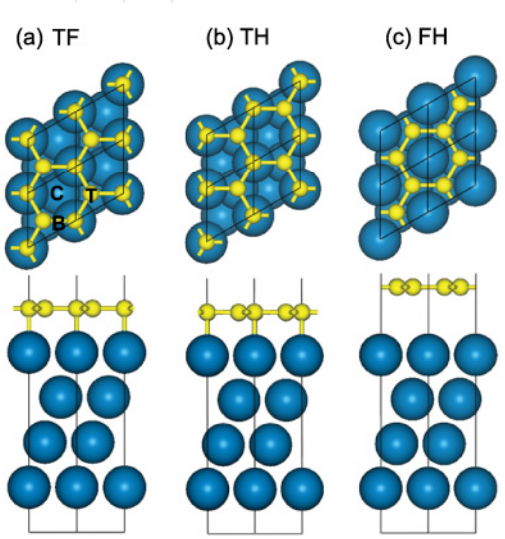

FIG. 1. (Color online) Three possible structures with C_{3v} symmetry for graphene on Ni(111) [or Cu(111)], shown in both top and side views. (a) top-fcc (TF), (b) top-hcp (TH), and (c) fcc-hcp (FH). Adsorbed water monomer can be placed on three different highly symmetric adsorption sites (in terms of oxygen's location) in these structures: (T) top, (B) bridge, and (C) center, with respect to graphene, which are labeled by black characters in panel (a). Yellow balls stand for C atoms, and blue for Ni (or Cu) atoms.

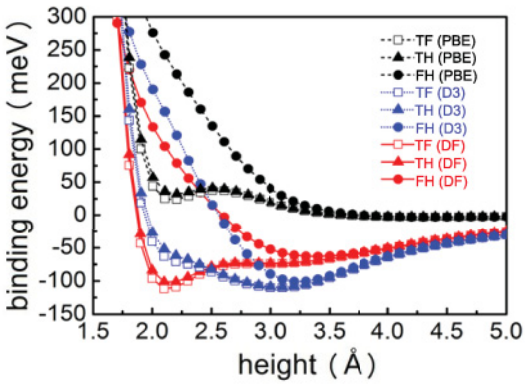

FIG. 2. (Color online) The binding energy versus height of the graphene sheet above Ni(111) in three adsorption structures, namely, TF, TH, and FH, using three different methods, namely, PBE, DFT-D3 (D3 for short), and optB86b-vdW (DF).

position, the C atoms are placed directly above the Ni atoms of the first (top site) and third (fcc site) layers. A similar terminology is used for the other two situations. In previous theoretical studies there have been discrepancies over which one of these structures is the most energetically favorable.[32,33] The TF interface with a binding distance of 2.1 Å is observed in most experimental studies,[31,34,35] suggesting that it is more stable than the other two structures.

We use the above fact to test the accuracy of the different exchange-correlation functionals for these systems. Table I shows our results using PBE, DFT-D3, and the optB86b-vdW approaches. For the three structures, PBE gives essentially no binding, and only a very shallow minimum of about 3 meV at >4 Å, which is within the numerical accuracy of the simulations. A careful examination of the binding energy versus height of the graphene sheet above the surface reveals an unbound (positive adsorption energy) local minimum at about 2.2 Å for both the TF and TH interfaces, as shown in Fig. 2. The presence of an unbound local minimum at 2.2 Å, consistent with previous PBE-based calculations of this system,[32,33] confirms that DFT at the GGA level is inappropriate for describing the weak van der Waals interactions in this system.

Moving to the DFT-D3 scheme, we find that DFT-D3 reduces the binding distances to 3.25–3.40 Å for the three structures, which are better than the results of the PBE functional, but still deviate significantly from the experimental binding distance of 2.1 Å. Using DFT-D3, the three structures are all bound by about 100–110 meV/carbon, with the TF configuration being the most stable, in agreement with experimental results.[35]

The optB86b-vdW scheme gives both reasonable binding distances and energies. In contrast to PBE and DFT-D3 results, for both the TF and TH interfaces, graphene is close to the Ni(111) surface at a perpendicular separation of 2.12–2.14 Å. This is within the typical range for Ni-C

TABLE I. Binding energy ($E_{G\text{-}M}$) and the average perpendicular distances (d) between graphene and the first layer of Ni(111) [or Cu(111)] for graphene on Ni(111) [or Cu(111)] in three adsorption structures, namely, top-fcc (TF for short), top-hcp (TH), and fcc-hcp (FH). Results with three different methods, namely, PBE, DFT-D3 (D3 for short), and optB86b-vdW (DF for short) are reported. $E_{G\text{-}M}$(D3) is decomposed into two parts, E^{D3} and E^{GGA}, while $E_{G\text{-}M}$(DF) is decomposed into E^{nlc} and the remainder (E^{r} for short). A negative (positive) E means that graphene is bound (unbound) to the Ni(111) surface.

	$E_{G\text{-}M}$(PBE) (meV)	d(PBE) (Å)	$E_{G\text{-}M}$(D3) (meV)	E^{D3} (meV)	E^{GGA} (meV)	d(D3) (Å)	$E_{G\text{-}M}$(DF) (meV)	E^{nlc} (meV)	E^{r} (meV)	d(DF) (Å)
Ni-TF	∼–3[a]	∼4.36	–107	–147	40	3.25	–112	–277	165	2.12
Ni-TH	∼–3	∼4.40	–106	–143	37	3.28	–103	–272	169	2.14
Ni-FH	∼–3	∼4.46	–97	–134	37	3.40	–63	–109	46	3.41
Cu-TF	∼–2	∼4.39	–113	–151	38	3.33	–67	–125	58	3.24
Cu-TH	∼–2	∼4.44	–113	–152	39	3.32	–66	–130	64	3.19
Cu-FH	∼–2	∼4.52	–106	–139	33	3.34	–61	–116	55	3.30

[a]"∼" is placed before all the PBE numbers, because PBE gives essentially no binding and only very shallow minima within the limits of the numerical accuracy of our simulations.

chemical bonds similar to other vdW-DF calculations,[22] and notably close to the 2.1 Å graphene-Ni(111) distance measured using low-energy electron diffraction (LEED).[35] In the TF configuration the graphene sheet is slightly closer to the surface than in the TH configuration (Table I and Fig. 2). On the other hand, the distance between graphene and the Ni(111) surface for the FH configuration is about 3.41 Å, suggesting a physisorption by optB86b-vdW. Using optB86b-vdW, the binding energies fall in the range from about 60 to 110 meV, with the TF model being the most stable, in agreement with experimental observations.[35] Thus, out of the three approaches considered, optB86b-vdW is the only one that predicts the correct adsorption configuration, and also yields a graphene-Ni distance that is in good agreement with available experimental data.

To further quantify the contribution from van der Waals interactions in graphene-metal binding, we have decomposed the binding energies obtained with the vdW-corrected methods (Table I). For the DFT-D3 approach we have split it into two parts, the GGA part, E^{GGA}, and the vdW correction, E^{D3}. E^{GGA} corresponds to the revPBE binding energies for the relaxed geometries from DFT-D3, which gives unbound results for all three structures with similar binding energies, somewhat similar to the PBE results. Because the binding distance for both the TF and TH interfaces is closer to the optimal vdW value than that of FH interface, E^{D3} for TF and TH is larger than that for FH, and then TF becomes the most stable after the D3 correction. We also decompose the binding energies obtained by optB86b-vdW into two parts: E^{nlc} and the remainder. The remainder also gives unbound results; with E^{nlc} correction, the order of stability of three structures changes and agrees with experimental observations.[35]

We have also calculated the binding energy of graphene on Cu(111) using the three methods (Table I), where optB86b-vdW again performs best by comparing to experimental results.[36] The three structures of graphene/Cu(111), TF, TH, and FH, all have a binding distance of 3.19–3.30 Å, implying physisorption, and an energy of −61 to −67 meV per C atom (in optB86b-vdW). The interaction between graphene and Cu(111) is weaker than the graphene-Ni(111) interaction, in accordance with previous work.[5,8] Therefore, we choose the most stable TF interface of graphene/Cu(111), which has a binding distance of 3.24 Å and energy of −67 meV, as the representative case for graphene/Cu(111).

From the above discussion, it is apparent that the optB86b-vdW approach is more suitable for describing the graphene/metal systems considered here than the PBE and DFT-D3 methods. Consequently, we use optB86b-vdW in all the subsequent calculations. In addition, we note that the three interface structures coincidentally correspond to three different domains of moiré superstructure of graphene on various metal surfaces. For instance, for graphene supported on Ru(0001),[15] local top-fcc and top-hcp adsorption sites are also observed as the lower and strongly bound regions, with local hcp-fcc regions as the higher and weakly bound region. These three interface arrangements also appear in some moiré superstructures of graphene/Ni(111) produced by lattice rotation. Therefore, the TF and FH graphene/Ni(111) interface may be used as models of the hollow (lower) and mound (higher) regions of a moiré superstructure,[12] considering that the TF and TH interfaces are very similar (Table I and Fig. 2).

B. Water monomer adsorption

We now explore the effect of water adsorption on the graphene/metal surfaces. We choose three surfaces as models, referred to as graphene/Ni-TF, graphene/Ni-FH, and graphene/Cu-TF, respectively, where Ni and Cu are the substrates on which graphene is directly grown, and TF and FH show the relative position of the graphene carbon atoms on these substrates as defined before (cf. Fig. 1). We intend to explore water adsorption on different domains of the moiré superstructure by comparing results of Ni-TF and Ni-FH, and the roles of different metal substrates by comparing Ni-TF and Cu-TF.

We first calculated water adsorption on free-standing graphene for comparison. The adsorption energies fall in a narrow range between −140 and −132 meV/water, and the adsorption heights between 3.33 and 3.35 Å (Table II), measured from the plane of graphene. The results for water on graphene with the optB86b-vdW functional are reasonable, only slightly larger than the upper end of the range of recent reference values computed with accurate explicitly correlated methods.[23,37–39]

The adsorption of a single water molecule on the model substrates is then investigated to reveal the nature of water-graphene/metal interaction. We employ a 5×5 supercell of graphene (50 C atoms, together with 25 metal atoms

TABLE II. Adsorption energies and distances of water monomer on free graphene, graphene/Ni-TF, graphene/Ni-FH, and graphene/Cu-TF obtained with the optB86b-vdW functional. Adsorbed water monomer can be placed in three highly symmetric adsorption sites (in terms of oxygen's location): (T) top, (B) bridge, and (C) center. For water monomer adsorption on a single layer of graphene, because two C atoms in a unit cell of graphene are identical, the T sites are all equivalent. With the metal substrate under graphene the T sites are no longer all equivalent, so there are two different T sites (T_1 and T_2) for water monomer adsorption on graphene/metal. The distances (d) are the perpendicular separations between the O atom of the water monomer and the surfaces.

	C site		B site		T_1 site		T_2 site	
	E (meV)	d (Å)	E (meV)	d (Å)	E (meV)	d (Å)	E (meV)	d (Å)
G	−140	3.33	−135	3.34	−132	3.35	−132	3.35
G/Ni-TF	−183	3.21	−176	3.26	−174	3.28	−173	3.28
G/Ni-FH	−158	3.29	−152	3.31	−149	3.31	−149	3.31
G/Cu-TF	−155	3.31	−151	3.33	−147	3.36	−145	3.36

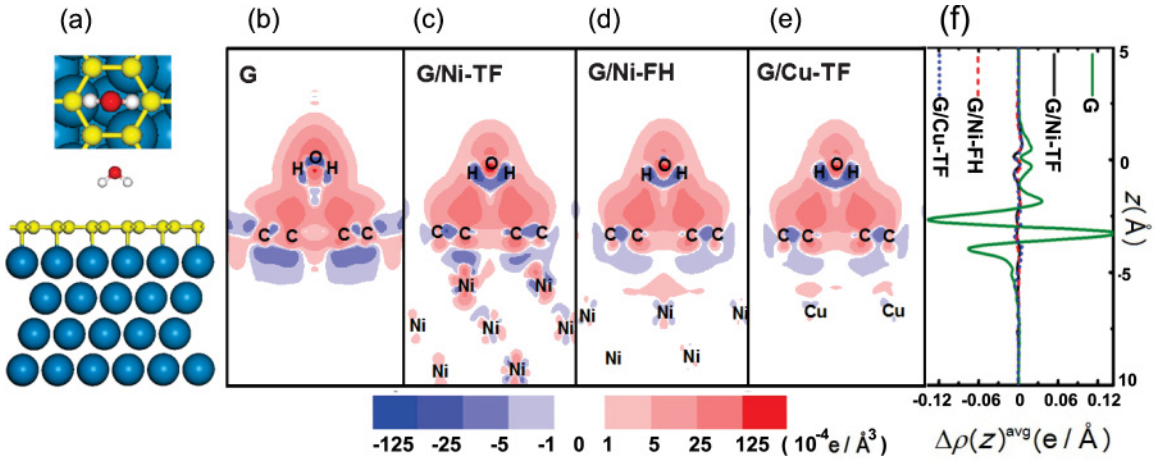

FIG. 3. (Color online) (a) The most stable adsorption structure of a water monomer on graphene/Ni-TF. In this structure the water is in a vertical orientation at the center of a C hexagon with the O-H bonds directed to two neighboring carbon atoms. Similar structures are seen for water on graphene, graphene/Ni-FH, and graphene/Cu-TF. Red balls represent the O atoms, white the H atoms, yellow the C atoms, and blue the Ni atoms. 2D slice of the charge density difference (obtained with the optB86b-vdW functional) for water monomer on (b) graphene, (c) graphene/Ni-TF, (d) graphene/Ni-FH, and (e) graphene/Cu-TF, through the plane of the adsorbed water molecule. (f) Plane-averaged electron density differences, $\Delta\rho^{\text{avg}}(z)$, of the four systems. The vertical position z is given relative to the O atom of water monomer (zero point). A (5×5) supercell of graphene was used, but only a portion of it is shown in panels (b)–(e).

substrate slab), large enough to eliminate significant water-water interactions between neighboring periodic images. By geometry optimization we find that water adsorption at the center of a carbon hexagon [the center site, Fig. 1(a)] is the most stable, where the water molecule stands vertically with two O-H bonds pointing toward two neighboring carbon atoms [Fig. 3(a)]. On graphene/Ni-TF, the adsorption energy is −183 meV with an O-C vertical distance of 3.21 Å (Table II). The adsorption energies of water at the other two sites are only slightly weaker. Specifically, water adsorption at the bridge (top) site [Fig. 1(a)] has an adsorption energy 7 meV (9 meV) smaller in magnitude, and a binding height 0.05 Å (0.07 Å) higher, than for the case at the center site.

For water monomer adsorption on graphene/Ni-FH and graphene/Cu-TF the adsorption energies are −158 meV and −155 meV, respectively, with bonding distances of 3.29 Å and 3.31 Å (Table II). Therefore, the energy difference for water adsorption on graphene/Ni-TF and on graphene/Ni-FH is 25 meV, similar to that for xenon on the mound and valley regions of graphene/Ru(0001)[15] (a difference of 9 meV). This suggests that water molecules prefer to adsorb on the hollow rather than on the mounds of moiré superstructures, and may self-assemble into ordered patterns on the metal-supported graphene moiré superstructures at low temperature. Such phenomena have been observed experimentally on a single layer of hexagonal boron nitride on Rh(111).[40] Moreover, water is still physisorbed, although the magnitude of the adsorption energy increases by 11%–31% when graphene is supported on the metal substrates.

To understand the electronic nature of the water-graphene/metal interaction, we display in Fig. 3 electron density differences, $\Delta\rho(\mathbf{r})$, of the nearby region of an adsorbed water monomer along the plane of the water monomer on graphene, graphene/Ni-TF, graphene/Ni-FH, and graphene/Cu-TF, respectively. For the water monomer on free-standing graphene, it is found that charge rearrangement is spatially quite diffuse. On the upper and lower surfaces of graphene, there are regions of electron density depletion, while electron accumulation is observed at the intermediate region between the water monomer and graphene, forming a bulge of electron gain. On graphene/Ni-TF, it is observed that the Ni atoms are affected by water adsorption. Although these atoms are at least 5.5 Å away from the water (counting Ni-O distances) a small charge redistribution in their vicinity (mainly of d_{z^2} and d_{xz} character) is observed. This interaction is quite long ranged, extending to a few layers of Ni atoms below the interface. The region of electron density gain above the water molecule becomes smaller and the bulge of electron accumulation becomes slightly larger, compared to the case of water on isolated graphene. In addition, the electron depletion region around graphene is slightly suppressed.

Moving to the weakly interacting graphene and metal surfaces, the features of the electron density redistribution plots are quite different. Although the d-orbital-like electron density redistribution also shows up in the case of water on graphene/Ni-FH, the magnitude is small and it decays rapidly below the interface. It diminishes after the second layer of Ni atoms. Charge redistribution is similar in the case of graphene/Cu-TF, but electron density changes around the substrate Cu atoms are even smaller. There is a second layer of electron accumulation just above the metal surface, which is not observed for water on free graphene or strongly bonded graphene. Therefore, a weak graphene-metal interaction (graphene/Ni-FH and graphene/Cu-TF) corresponds to weaker water binding, relative to the case of the strong graphene-metal interaction (graphene/Ni-TF).

Figure 3(f) shows the plane-integrated charge density difference along the cross sections (parallel to graphene) of the model system. For water monomer on free graphene, it displays a charge polarization of graphene due to water

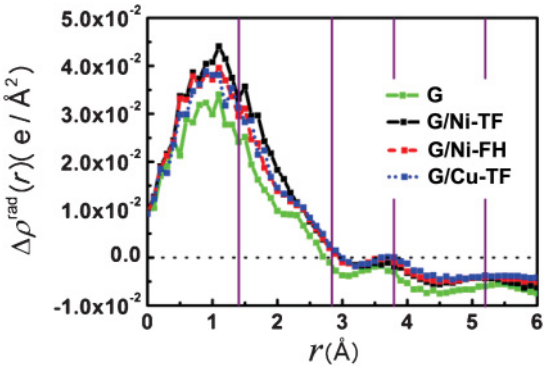

FIG. 4. (Color online) The lateral radial electron density differences in the proximity of graphene for four systems. The green solid line represents free graphene, the black solid line graphene/Ni-TF, the red dashed line graphene/Ni-FH, and the blue dotted line graphene/Cu-TF. r is the lateral radial distance from the origin of the x-y plane, which is set to the location of O in water molecule. The purple bold lines indicate the positions of C atoms in the graphene in the model system.

adsorption, a $-/+/-$ sequence of charge difference as one moves from the lower surface of graphene to the upper one. But for the other three systems with the metal substrate, the charge oscillation is one magnitude smaller, compared to free graphene. However, the absence of significant vertical oscillations in $\Delta\rho(z)$ for the entire cell does not mean the absence of a density response upon the approach of water to graphene in the presence of a metal substrate. Quite to the contrary, the adsorption-induced lateral density oscillations in graphene are enhanced in the presence of the metal substrates (see the supporting information for more details Ref. 41). To see this, we calculate the lateral radial density difference in the proximity of graphene, defined as

$$\Delta\rho^{\mathrm{rad}}(r) = \frac{1}{2\pi r}\frac{d}{dr}\int_{z_0-\delta/2}^{z_0+\delta/2} dz \int_{x^2+y^2\leqslant r^2} dxdy\Delta\rho(x,y,z), \tag{8}$$

where z_0 corresponds to the height of graphene, the origin of the x-y plane is set to the location of O in the water molecule, with r being the distance from the origin, and $\delta = 3.3$ Å, corresponding to the interlayer separation in bulk graphite. The lateral density difference is shown in Fig. 4. With or without the metal substrate, the lateral-induced density responses show buildups of electrons near the "legs" (H atoms) of water, located around the position of the nearest C atoms on graphene. There are several weak peaks corresponding to the position of the C atoms, showing the charge rearrangement of the C atoms after water adsorption. For water monomer adsorption on graphene/Ni-TF, graphene/Ni-FH, and graphene/Cu-TF, the first large peaks are systematically larger than free-standing graphene. The density difference in all cases turns negative (electron depletion) at larger r: at ∼2.7 Å for free-standing graphene and at ∼3 Å when a metal substrate is present. This finding is connected to the Friedel oscillation (FO),[42,43] the spatially oscillatory density response of an interacting electron gas to an impurity. In two dimensions, the FO decays as $1/r^2$. In pristine graphene, the analytic form of the FO decays at large distance as $1/r^3$.[43] Our model is not large enough to see the scaling behavior of the density at very large distances.

The presence of large electron pockets in the neighborhood of the H-down water should enhance the physisorption energy Coulombically. The peak for graphene/Ni-TF is the highest, and the peaks for graphene/Ni-FH and graphene/Ni-TF are slightly lower, while the peaks for graphene are lowest. A Fermi sea in the neighborhood of graphene clearly modifies the dielectric environment.[44,45] With the metal substrate under graphene, the screening effect is stronger than the one for the free-standing graphene. The stronger screening effect makes a larger electron density build-up, in response to a polar molecule. Consequently, the presence of a metal substrate enhances the binding of physisorption of a polar molecule on graphene. The heights of induced density peaks are consistent with the increments of adsorption energies. As a matter of accounting, the electron density build-up comes *not* from the metal underneath, but mainly from the electrons of graphene itself, for the electron deficit (surplus) in metals is small and superficial.

To look into the chemical nature of the molecular interaction between water and the supported graphene, Fig. 5 shows the sites of the $1b_1$ orbital (HOMO) of water and projected density of states (PDOS) onto the six C atoms which are closest to the adsorbed water. We found that the PDOS on C shows a nice linear feature around its minimum (the Dirac point), which characterizes the electronic structure of graphene, except for graphene/Ni-TF in Fig. 5(b). This feature is absent in the graphene/Ni-TF case due to the strong chemical bonding between graphene and Ni(111). For the cases of graphene/Ni-FH and graphene/Cu-TF, the weak graphene-metal interaction not only maintains the linear PDOS feature of graphene, but also presents a hole (electron) doping effect in graphene, manifesting as a shift of Fermi level below (above) the Dirac point.

The $1b_1$ orbital of water is very sensitive to the bonding environment. Relative to the Fermi level of the system, it shifts in the range from −2.29 eV (on graphene/Ni-FH) to −3.11 eV (on graphene/Ni-TF). The shift to the Dirac point is less pronounced. Compared to its energy for water on isolated graphene, the $1b_1$ orbital shifts by −0.59 eV on graphene/Ni-TF, +0.23 eV on graphene/Ni-FH, and −0.09 eV on graphene/Cu-TF, where the extent of the shift is consistent with the changes of the adsorption energy.

Note also that the PDOS of selected C atoms changes slightly upon water adsorption, shown in Fig. 5. This demonstrates that there is a response from the orbitals of graphene to water adsorption on free graphene, graphene/Ni-FH, and graphene/Cu-TF to a small extent, in spite of the molecule only being physisorbed. However, it does not change for water on graphene/Ni-TF, possibly because the strong graphene-metal chemical contact makes graphene less sensitive to water adsorption.

C. Adsorption of water overlayers

We now go beyond the monomer and investigate the influence of water overlayers on the electronic interactions between graphene and the metal surface. To this end, we construct model icelike bilayer structures on the surface of graphene/Ni(111) and graphene/Cu(111). Two ice bilayer

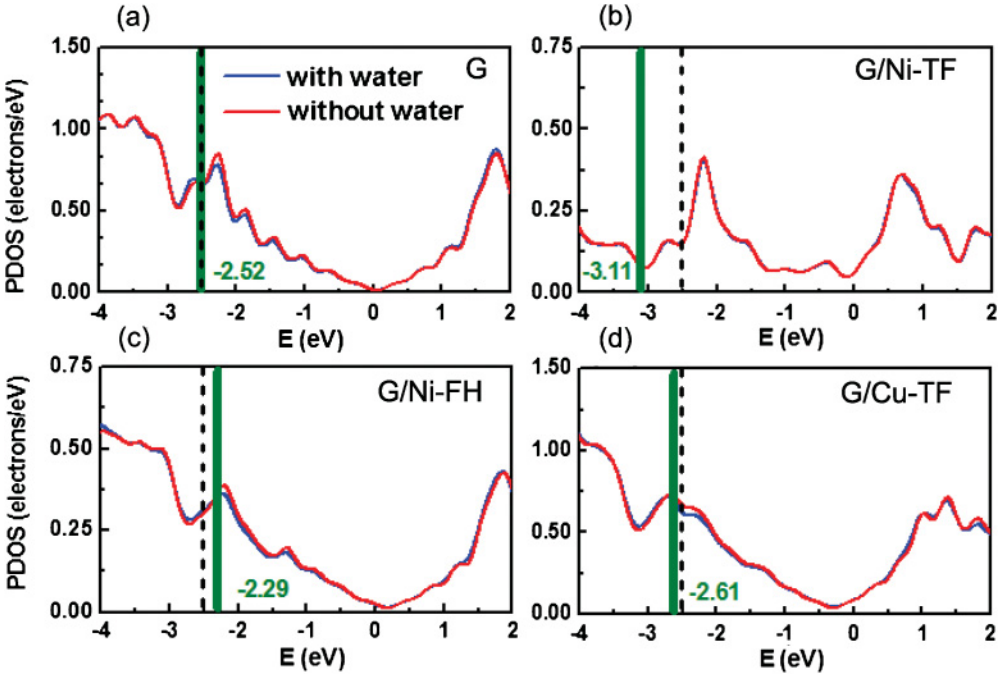

FIG. 5. (Color online) Projected density of states (PDOS) onto the adsorbed water monomer and the C atoms of graphene closest to the monomer for water monomer adsorption on (a) graphene, (b) graphene/Ni-TF, (c) graphene/Ni-FH, and (d) graphene/Cu-TF. The blue and red curves represent the PDOS projected onto the C atoms of the four surfaces with and without water adsorption, respectively. The green bold lines and the numbers nearby indicate the highest occupied molecular orbital (HOMO) of the water monomer on the four surfaces, while the dashed lines indicate the HOMO of the water monomer on free graphene for comparison. Energy scales are zeroed to E_F. For the Ni systems only spin-up states are shown; the spin-down states are similar and not shown.

models were considered. In the first model, the non-hydrogen-bonded OH group points toward (H-down configuration) the surface, whereas in the other model OH groups point away from (H-up) the surface. For simplicity we choose the $(\sqrt{3} \times \sqrt{3})R30^\circ$ graphene supercell shown in Figs. 6(a) and 6(b), similar to what has been used before in previous theoretical studies for ice bilayers on metal surfaces.[46,47] Although there is no experimental confirmation of the formation of an icelike bilayer structure on graphene, and the existence of bilayer structures at surfaces is controversial,[48] it is a useful and simple model from which we can gain semiquantitative insights into the role of water overlayers in tailoring the electronic properties of metal-supported graphene. The adsorption energies of H-up and H-down water bilayers on free graphene, graphene/Ni-TF, graphene/Ni-FH, and graphene/Cu-TF are shown in Table III. The adsorption energy differences between H-up and H-down ice bilayers on each surface are all very small (all smaller than 7 meV/H_2O). Adsorption energies of the H-up bilayers are all slightly more stable than for H-down bilayers, in contrast to previous results of ice bilayer adsorption on free graphene without vdW corrections.[49]

Band structures for the H-down ice bilayer on free graphene, graphene/Ni-TF, graphene/Ni-FH, and graphene/Cu-TF are shown in Fig. 6. The band structures for the H-up bilayers are similar and not shown. The Dirac conical point lies at the Γ point, since in the $(\sqrt{3} \times \sqrt{3})R30^\circ$ supercell, the K and K' points of the Brillouin zone are folded back to the Γ point. Water adlayers on isolated graphene do not destroy the shape of the Dirac cone, nor do they shift the Fermi level. Only a small gap of ~40 meV opens up, whose center coincides with the Fermi level [Fig. 6(c)]. It indicates that water adsorption indeed opens a small band gap in graphene, which can survive at room temperature.[50]

Prior to water adsorption, the graphene/Ni-TF interface shows a large band-gap opening and strong band hybridization between graphene and the Ni(111) substrate. Water overlayer adsorption does not change the band structure, except for a tiny band shift, 15 meV on average at Γ, for both H-down and H-up bilayers. We infer that the strong carbon-metal hybridization pins the levels of graphene π and π^* bands in this case.

As stated before, graphene is p doped for graphene/Ni-FH, with the Fermi level located about 60 meV below the Dirac point. The H-down ice bilayer on such a surface shifts the Fermi level upwards by about 30 meV, while adsorption of the H-up bilayer shifts the Fermi level downwards by about 80 meV, now at about 140 meV lower than the Dirac point. As

TABLE III. Adsorption energies and distances of H-up and H-down water bilayers on free graphene, graphene/Ni-TF, graphene/Ni-FH, and graphene/Cu-TF obtained with the optB86b-vdW functional. The distances (d) are the perpendicular separations between the O atoms of the lower water layer and the graphene surfaces.

		G	G/Ni-TF	G/Ni-FH	G/Cu-TF
H-up	E (meV)	−542	−565	−553	−561
	d (Å)	3.17	3.01	3.09	3.07
H-down	E (meV)	−540	−558	−550	−559
	d (Å)	3.27	3.25	3.33	3.34

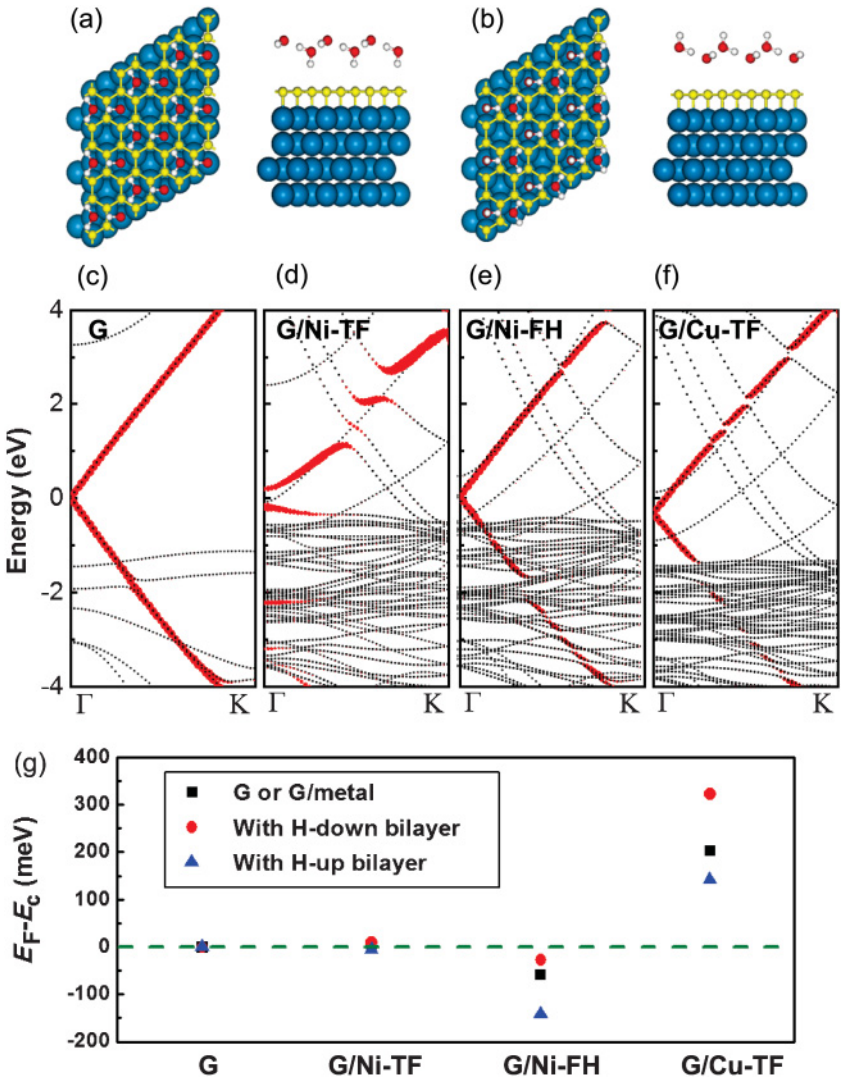

FIG. 6. (Color online) Structures of (a) H-down and (b) H-up water bilayers in the $(\sqrt{3} \times \sqrt{3})R30^\circ$ symmetry on graphene/Ni-TF. Red balls represent O atoms, white the H atoms, yellow the C atoms, and blue the Ni atoms. Band structures of the H-down bilayer on (c) graphene, (d) graphene/Ni-TF, (e) graphene/Ni-FH, and (f) graphene/Cu-TF. The red dots on certain bands indicate states of p_z character, with the size of the dot proportional to the extent of p_z character. The energy scales are shifted with respect to E_F taken as the zero of energy. For the Ni systems, only the spin-up state is shown as the spin-down state is similar. (g) The Fermi level relative to the conical point, E_F–E_C, for the four surfaces with and without the H-up and H-down bilayers. Black squares are for the clean substrates, red circles are for the H-down bilayer, and the blue triangles are for H-up bilayer. For graphene/Ni-TF, the conical point is destroyed; the reference is instead placed on the average value at Γ of the two graphene bands to look into the Fermi level shift.

with the free graphene case, the adsorption of water overlayers also increases the band gap by 20 meV. The shift is also observed for the Cu-TF case: On Cu-TF, graphene is *n* doped with the Fermi level about 200 meV higher than the Dirac point; however, the H-down ice bilayer shifts the Fermi level upwards by 120 meV, while the H-up ice bilayer shifts it downwards by 60 meV. These results are summarized in Fig. 6(g). These shifts can be explained based on the effect of the bilayer electrostatic field, as we will discuss below.

Interestingly, the interactions between the water overlayers and graphene, and between the physisorbed graphene and the metal surface are coupled. Without the metal substrate, H-down ice bilayer does not induce the distinct shift of the Fermi level. However, on weakly interacting metal substrates such as Ni-FH and Cu-TF, the H-down ice bilayer shifts the graphene Fermi level upwards. With the H-down bilayer adsorption, the metal substrates are polarized by the electric field induced by the ice bilayer,[51,52] and as a result the on-site energy of electrons of both graphene and the metal substrate are both shifted downward. But as graphene is closer to the ice overlayer, its energy level shift is larger than that of the metal. This leads to band realignment where the Dirac point of graphene moves downward relative to the Fermi level, mimicking electron doping. When the ice overlayer has the H-up configuration, the electric field felt by graphene and the metal substrate is just the opposite, producing a hole doping effect with reference to the graphene-metal composite. This way, the three components of the water-graphene-metal composite are correlated in their mutual interactions: Both water and the metal substrates play a role in modifying the electronic structure of graphene, and they themselves are mutually influenced via graphene as a bridge. The chemisorption of graphene on Ni-TF, on the other hand, makes graphene insensitive to ice layers. Simply put, depending on its local orientation, the ice bilayer either moves up or down the Fermi level of graphene with respect to the Dirac point, thus altering the electron doping level of the graphene/metal interface.

IV. CONCLUSIONS

We have investigated the interaction between water and metal-supported graphene. Both water monomer and water overlayer adsorption (using simple bilayer models) was considered. Among the different methods tested in describing graphene-metal interactions, the optB86b-vdW functional developed recently by Klimeš *et al.*[26] gives the most

reasonable structures and energies. We find that the presence of a metal substrate enhances the induced lateral density response in graphene to the dipole of the adsorbed water. This enhancement of lateral density response leads water to bind more strongly to graphene on a metal substrate, relative to free-standing graphene. With metal substrates under graphene, the adsorption energies of water monomer increase by 11%∼31%, but they have only a maximum value of 183 meV. Moreover, the adsorption energies of the ice bilayer increase just by ∼20 meV, while the adsorption energies are ∼500 meV due to the formation of the H-bond interactions between water molecules. Therefore, though the adsorption energies increase with metal substrates, graphene/metal is still hydrophobic (knowing how inexact, albeit very useful, the meaning of hydrophobicity can be), weaker than the interaction between water and metal substrate directly without graphene, and weaker than the interaction between water molecules.[46]

We also show that water adsorption and interaction with the metal substrate are two effective ways to modify the electronic structure of graphene. For the strong chemical bonding between graphene and the metal, as represented by the graphene/Ni-TF case, the metal substrate largely changes the conical band structure of graphene, opens a gap of ∼400 meV, and pins the graphene bands making them insensitive to water adsorption. For the weaker physical contacts between graphene and metals, such as the Ni-FH and Cu-TF systems, we found that water and the metal substrates have a combined correlated effect on electron doping of graphene. Without the metal substrates, water hardly changes the Fermi level of graphene. However, on weakly interacting metal substrates, the H-up and H-down icelike bilayer shift the Fermi level of graphene towards or away from the Dirac point by ∼100 meV. These results illustrate the potential for codoping effects, which may find potential use in the development of next generation graphene-based electronic devices.

ACKNOWLEDGMENTS

The work was supported by NSFC (Projects No. 10974238, No. 91021007, and No. 11174009) and MOST of China. A.M. is supported by the European Research Council and J.K. has received support from UCL and EPSRC through the PhD+ scheme. S.M. acknowledges supports from NSFC (Grant No. 11074287) and CAS.

*jfeng11@pku.edu.cn

[1] J. Wintterlin and M. L. Bocquet, Surf. Sci. **603**, 1841 (2009).
[2] Y. Pan, H. G. Zhang, D. X. Shi, J. T. Sun, S. X. Du, F. Liu, and H. J. Gao, Adv. Mater. **21**, 2777 (2009).
[3] S. Y. Kwon, C. V. Ciobanu, V. Petrova, V. B. Shenoy, J. Bareno, V. Gambin, I. Petrov, and S. Kodambaka, Nano Lett. **9**, 3985 (2009).
[4] K. S. Novoselov, A. K. Geim, S. V. Morozov, D. Jiang, M. I. Katsnelson, I. V. Grigorieva, S. V. Dubonos, and A. A. Firsov, Nature **438**, 197 (2005).
[5] G. Giovannetti, P. A. Khomyakov, G. Brocks, V. M. Karpan, J. van den Brink, and P. J. Kelly, Phys. Rev. Lett. **101**, 026803 (2008).
[6] Y. Murata, E. Starodub, B. B. Kappes, C. V. Ciobanu, N. C. Bartelt, K. F. McCarty, and S. Kodambaka, Appl. Phys. Lett. **97**, 143114 (2010).
[7] V. M. Karpan, G. Giovannetti, P. A. Khomyakov, M. Talanana, A. A. Starikov, M. Zwierzycki, J. van den Brink, G. Brocks, and P. J. Kelly, Phys. Rev. Lett. **99**, 176602 (2007).
[8] P. A. Khomyakov, G. Giovannetti, P. C. Rusu, G. Brocks, J. van den Brink, and P. J. Kelly, Phys. Rev. B **79**, 195425 (2009).
[9] Q. S. Ran, M. Z. Gao, X. M. Guan, Y. Wang, and Z. P. Yu, Appl. Phys. Lett. **94**, 103511 (2009).
[10] Z. P. Xu and M. J. Buehler, J. Phys. Condens. Matter **22**, 485301 (2010).
[11] C. Gong, G. Lee, B. Shan, E. M. Vogel, R. M. Wallace, and K. Cho, J. Appl. Phys. **108**, 123711 (2010).
[12] O. V. Yazyev and A. Pasquarello, Phys. Rev. B **82**, 045407 (2010).
[13] A. T. N'Diaye, S. Bleikamp, P. J. Feibelman, and T. Michely, Phys. Rev. Lett. **97**, 215501 (2006).
[14] M. Sicot, S. Bouvron, O. Zander, U. Rudiger, Y. S. Dedkov, and M. Fonin, Appl. Phys. Lett. **96**, 093115 (2010).
[15] T. Brugger, S. Gunther, B. Wang, J. H. Dil, M. L. Bocquet, J. Osterwalder, J. Wintterlin, and T. Greber, Phys. Rev. B **79**, 045407 (2009).
[16] G. Kresse and J. Hafner, Phys. Rev. B **47**, 558 (1993).
[17] G. Kresse and J. Furthmuller, Phys. Rev. B **54**, 11169 (1996).
[18] G. Kresse and D. Joubert, Phys. Rev. B **59**, 1758 (1999).
[19] H. J. Monkhorst and J. D. Pack, Phys. Rev. B **13**, 5188 (1976).
[20] G. Makov and M. C. Payne, Phys. Rev. B **51**, 4014 (1995).
[21] J. Neugebauer and M. Scheffler, Phys. Rev. B **46**, 16067 (1992).
[22] I. Hamada and M. Otani, Phys. Rev. B **82**, 153412 (2010).
[23] J. Ma, A. Michaelides, D. Alfe, L. Schimka, G. Kresse, and E. G. Wang, Phys. Rev. B **84**, 033402 (2011).
[24] S. Grimme, J. Antony, S. Ehrlich, and H. Krieg, J. Chem. Phys. **132**, 154104 (2010).
[25] J. Klimeš, D. R. Bowler, and A. Michaelides, J. Phys. Condens. Matter **22**, 022201 (2010).
[26] J. Klimeš, D. R. Bowler, and A. Michaelides, Phys. Rev. B **83**, 195131 (2011).
[27] M. Dion, H. Rydberg, E. Schroder, D. C. Langreth, and B. I. Lundqvist, Phys. Rev. Lett. **92**, 246401 (2004).
[28] G. Roman-Perez and J. M. Soler, Phys. Rev. Lett. **103**, 096102 (2009).
[29] J. P. Perdew, K. Burke, and M. Ernzerhof, Phys. Rev. Lett. **77**, 3865 (1996).
[30] P. Haas, F. Tran, and P. Blaha, Phys. Rev. B **79**, 085104 (2009).
[31] Y. S. Dedkov and M. Fonin, New J. Phys. **12**, 125004 (2010).
[32] G. Bertoni, L. Calmels, A. Altibelli, and V. Serin, Phys. Rev. B **71**, 075402 (2005).
[33] M. Fuentes-Cabrera, M. I. Baskes, A. V. Melechko, and M. L. Simpson, Phys. Rev. B **77**, 035405 (2008).
[34] S. Böttcher, M. Weser, Y. S. Dedkov, K. Horn, E. N. Voloshina, and B. Paulus, Nanoscale Res. Lett. **6**, 214 (2011).
[35] Y. Gamo, A. Nagashima, M. Wakabayashi, M. Terai, and C. Oshima, Surf. Sci. **374**, 61 (1997).
[36] A. M. Shikin, V. K. Adamchuk, and K. H. Rieder, Phys. Solid State **51**, 2390 (2009).

[37]M. Rubeš, P. Nachtigall, J. Vondrášek, and O. Bludský, J. Phys. Chem. C **113**, 8412 (2009).
[38]K. D. Jordan, G. R. Jenness, and O. Karalti, Phys. Chem. Chem. Phys. **12**, 6375 (2010).
[39]E. Voloshina, D. Usvyat, M. Schutz, Y. Dedkov, and B. Paulus, Phys. Chem. Chem. Phys. **13**, 12041 (2011).
[40]H. F. Ma, T. Brugger, S. Berner, Y. Ding, M. Iannuzzi, J. Hutter, J. Osterwalder, and T. Greber, Chem. Phys. Chem. **11**, 399 (2010).
[41]See Supplemental Material at http://link.aps.org/supplemental/10.1103/PhysRevB.85.085425 for a further discussion on Fig. 3(f).
[42]N. W. Ashcroft and N. D. Mermin, *Solid State Physics* (Brooks/Cole, Belmont, CA, 1976) pp. 343.
[43]V. Cheianov and V. I. Fal'ko, Phys. Rev. Lett. **97**, 226801 (2006).
[44]J. M. Pitarke, V. U. Nazarov, V. M. Silkin, E. V. Chulkov, E. Zaremba, and P. M. Echenique, Phys. Rev. B **70**, 205403 (2004).
[45]J. Yan, K. S. Thygesen, and K. W. Jacobsen, Phys. Rev. Lett. **106**, 146803 (2011).
[46]S. Meng, E. G. Wang, and S. W. Gao, Phys. Rev. B **69**, 195404 (2004).
[47]A. Michaelides, A. Alavi, and D. A. King, Phys. Rev. B **69**, 113404 (2004).
[48]A. Hodgson and S. Haq, Surf. Sci. Rep. **64**, 381 (2009).
[49]O. Leenaerts, B. Partoens, and F. M. Peeters, Phys. Rev. B **79**, 235440 (2009).
[50]F. Yavari, C. Kritzinger, C. Gaire, L. Song, H. Gullapalli, T. Borca-Tasciuc, P. M. Ajayan, and N. Koratkar, Small **6**, 2535 (2010).
[51]T. O. Wehling, A. I. Lichtenstein, and M. I. Katsnelson, Appl. Phys. Lett. **93**, 202110 (2008).
[52]J. Moser, A. Verdaguer, D. Jimenez, A. Barreiro, and A. Bachtold, Appl. Phys. Lett. **92**, 123507 (2008).